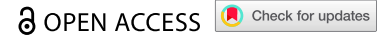



BRIEF REPORT



ALCAM-mediated cDC1 CD8 T cells interactions are suppressed in advanced lung tumors

Luciano G. Morosi^a, Giulia M. Piperno^a, Lucía López^a, Roberto Amadio^a, Sonal Joshi^a, Alessandra Rustighi^{b,c}, Giannino Del Sal^{b,c,d}, and Federica Benvenuti^a 

^aCellular Immunology, International Centre for Genetic Engineering and Biotechnology (ICGEB), Trieste, Italy; ^bDepartment of Life Sciences, University of Trieste, Trieste, Italy; ^cCancer Cell Signaling, International Centre for Genetic Engineering and Biotechnology (ICGEB), Trieste, Italy; ^dIFOM ETS, The AIRC Institute of Molecular Oncology, Milan, Italy

ABSTRACT

Conventional type 1 dendritic cells (cDC1) are critical regulators of anti-tumoral T-cell responses. The structure and abundance of intercellular contacts between cDC1 and CD8 T cells in cancer tissues is important to determine the outcome of the T-cell response. However, the molecular determinants controlling the stability of cDC1-CD8 interactions during cancer progression remain poorly investigated. Here, we generated a genetic model of non-small cell lung cancer crossed to a fluorescent cDC1 reporter (KP-XCR1^{VENUS}) to allow the detection of cDC1-CD8T cell clusters in tumor tissues across tumor stages. We found that cDC1-CD8 clusters are abundant and productive at the early stages of tumor development but progressively diminish in advanced tumors. Transcriptional profiling and flow cytometry identified the adhesion molecule ALCAM/CD166 (Activated Leukocyte Cell Adhesion Molecule, ligand of CD6) as highly expressed by lung cDC1 and significantly downregulated in advanced tumors. Analysis of human datasets indicated that *ALCAM* is downregulated in non-small cell lung cancer and its expression correlates to better prognosis. Mechanistically, triggering ALCAM on lung cDC1 induces cytoskeletal remodeling and contact formation whereas its blockade prevents T-cell activation. Together, our results indicate that ALCAM is important to stabilize cDC1-CD8 interactions at early tumor stages, while its loss in advanced tumors contributes to immune evasion.

ARTICLE HISTORY

Received 21 February 2024
Revised 10 June 2024
Accepted 11 June 2024

KEYWORDS

ALCAM; cDC1; immunological synapse; lung cancer; NSCLC

Introduction

The presentation of tumor-derived antigens by antigen-presenting cells is a key factor in priming T cells in lymph nodes and maintaining effector functions and polarization of T cells in tumor tissues. Type 1 dendritic cells (cDC1) are uniquely efficient in capturing and cross-presenting cancer antigens to CD8 T cells and their function and regulatory mechanism in lung cancer have been intensely investigated.¹⁻⁴ For efficient transmission of signal 1 (MHC-peptide complexes), signal 2 (costimulatory molecules) and signal 3 (instructing cytokines), T cells and DCs must establish a functional adhesive structure, the immunological synapse (IS), to support proper inter-cellular communication.^{5,6} *Ex vivo* analysis identified complex and dynamic reorganization of the T cell side of the immunological synapse, encompassing stabilization by adhesion molecules, recruitment of cytoskeletal components and membrane receptors, spatial re-organization of signaling microclusters, and polarization of secretory vesicles.^{7,8} Symmetrically, on the DC side, contact formation induces spatial reorganization of membrane receptors,⁹ cytoskeletal regulators,^{10,11} and secretory vesicles,^{12,13} in addition to epigenetic and transcriptional remodeling.¹⁴ More recently, clusters of immune cells in tumor tissues are beginning to be characterized, unveiling the local determinants and composition of immune hubs that control anti-tumoral responses, locally in

tumor tissues.^{15,16} Further data identified triads composed of CD4, CD8 T cells and DCs as predictors of responses to checkpoint blockade.^{17,18} Intra-tumoral resident cDC1 actively controls the formation of these hubs, by attracting CD8 T cells to the stromal tumor regions through CXCL9 and CXCL10 and promoting the expansion of tumor-specific TCF1⁺ stem-like CD8 T cells,¹⁹ a mechanism that was recently shown to be impaired by prostaglandin E2 (PGE2).²⁰ Given the emerging relevance of immune interacting hubs in cancer tissues, understanding the molecular determinants implicated in controlling the stability of cDC1-CD8 T cell interactions and their changes during tumor progression has become an important open question.

Here, we modified a genetic model of non-small cell lung cancer (NSCLC) that recapitulates features of the human disease²¹ to introduce a cDC1-specific fluorescent reporter and explore their ability to establish productive interaction with CD8 T cells, at two well-defined stages of tumor development. By combining tissue imaging, transcriptional analysis, and assays of cDC1-CD8 T cell interactions *ex-vivo*, we found that the adhesion molecule ALCAM/CD166 is highly expressed on cDC1 in early tumors and it contributes to stabilize contacts and to promote full T cell activation. Conversely, ALCAM is strongly downregulated in late tumors cDC1, suggesting that loss of adhesion

molecules contributes to impair the ability to induce CD8 T cell activation.

Materials and methods

Mice

Mice strains used in this study were maintained in sterile isolators at the International Centre for Genetic Engineering and Biotechnology (ICGEB) animal BioExperimentation facility. Wild-type C57BL/6 animals were purchased from ENVIGO Laboratories. XCR1-Venus ($XCR1^{Venus/+}$)²² mice were kindly provided by Dr. Wolfgang Kastenmuller (University of Wuerzburg, Germany). Mice lines B6.129P2- $Trp53^{tm1Brn/J}$ ($p53^{LoxP}$, $Trp53^{fl/fl}$) and B6.129S4- $Kras^{tm4Tyj/J}$ ($Kras^{LSL-G12D}$) were obtained from The Jackson Laboratory (cod 008462 and 008179, respectively) and initially crossed to obtain the KP inducible mouse line ($Kras^{LSL-G12D/+}$; $Trp53^{fl/fl}$). KP-XCR1^{Venus} strain ($Kras^{LSL-G12D/+}$; $Trp53^{fl/fl}$; $XCR1^{Venus/+}$) was obtained by crossing the KP and XCR1-Venus colonies. OT-I C57BL/6-Tg(Tcra-V2/Tcrb-V5) animals were from Jackson Laboratories. OT-I^{TdTomato} mice were a kind gift of Dr. Kastenmuller. The study was approved by ICGEB's board for animal welfare and authorized by the Italian Ministry of Health (approval number 459/2022-PR, issued on 22/07/2022). Animal care and treatment were conducted under national and international laws and policies (European Economic Community Council Directive 86/609; OJL 358; December 12, 1987). All experiments were performed in accordance with the Federation of European Laboratory Animal Science Association (FELASA) institutional guidelines and the Italian law.

Induction of lung tumors

We used two mouse models of lung adenocarcinoma: autochthonous and transplantable.

In the autochthonous model, 8 to 10 weeks old KP or KP-XCR1^{Venus} male mice were inoculated intratracheally with 2.5×10^7 infectious particles of a replication-deficient adenoviral vector carrying the Cre recombinase gene under the CMV strong promoter (Ad-CMV-iCre, Vector Biolab, Cat# 1045), in order to induce tumor nodules in the lung. Mice were sacrificed after either 4 or 8 weeks post-adenovirus inoculation. In the transplantable model, the KP cell line LG1233 (kindly provided by Dr. Tyler Jacks) was maintained in complete DMEM media (Gibco, Cat# 21885–025) 10% fetal bovine serum (FBS) as previously described,³ and routinely tested for mycoplasma contamination. In order to induce lung tumor nodules in 8 to 10 weeks old WT or XCR1-Venus male mice 50,000 KP cells were injected intravenously in 100 μ L sterile PBS. Mice were sacrificed after either 8 or 28 days post-tumor inoculation. Tumor formation in lung tissues was assessed as follows: after sacrifice, healthy and tumor-bearing mice were intracardiac perfused with sterile PBS to remove the vascular component from lungs. Tissues were then harvested and fixed in formaldehyde 10% over-night (ON), and paraffin embedded following standard procedure. Five-micrometer consecutive sections were dewaxed, rehydrated, and stained with the

hematoxylin/eosin (H&E; Bio-Optica, Cat# 21-A140E). Images were acquired in a Leica DFC450 C microscope.

Ex vivo cDC1-CD8 T-cell conjugates

Sorted lung cDC1 were loaded with 10 nM MHC class I-restricted OVA peptide (OVA_{257–264}, SIINFEKL; Invivogen, Cat# vac-sin) in complete IMDM media (Gibco, Cat# 31980–022) 10% FBS for 1.5 hours at 37°C in a Eppendorf tube. Afterward, they were plated in fibronectin-coated round coverslips for 30 minutes at 37°C. After washing to remove not attached cells, naïve or effector CFSE-labeled OT-I cells (2 μ M CFSE; BioLegend, Cat# 423801) were added to coverslips in complete RPMI media (Gibco, Cat# 72400–021) 10% FBS for 30 minutes at 37°C (1:1, cDC1:OT-I ratio). After incubation, cells were washed with PBS and fixed in PBS 4% PFA for 15 minutes at RT. Afterward, the cells were permeabilized and blocked in Blocking buffer (PBS, 0.2% BSA, 0.05% saponin, 5% horse serum) for 40 minutes at RT. Then, cells were washed with PBS for 5 minutes at RT and F-actin was stained with Phalloidin-AF555 (Invitrogen, Cat# A34055) in Blocking buffer for 30 minutes at RT. After washing with PBS for 5 minutes at RT, nuclei were stained with Hoechst 33,342 in PBS for 20 minutes at RT. Lastly, coverslips were washed twice with PBS for 2 minutes at RT and mounted with Mowiol 40–88. Confocal microscopy images were acquired and analyzed as previously described.

Lung cDC1-beads conjugates

Sorted lung cDC1 were plated in fibronectin-coated round coverslips for 30 minutes at 37°C, in complete IMDM media 10% FBS with 1 μ M SiR-actin/10 μ M verapamil (SiR-actin kit; Spirochrome AG, Cat# SC001). After washing to remove the unattached cells, recombinant mouse CD6-Fc chimera (rCD6 (Fc); R&D Systems, Cat# 727-CD-100)-coated or recombinant human IgG1 Fc molecule (rFc; R&D Systems, Cat# 110-HG-100)-coated beads were added to coverslips in complete IMDM media with SiR-actin/verapamil, for 30 minutes at 37°C (3:1, bead:cDC1 ratio). After incubation, cells were washed once with cold PBS and incubated with rat anti-mouse ICAM-1-FITC (eBioscience, Cat# 11-0541-81) antibody in FACS buffer with 10 μ M verapamil for 60 minutes at 4°C. Afterward, the cells were washed with PBS and fixed in PBS 1% PFA for 15 minutes at RT, followed by permeabilization and blocking in Blocking buffer (PBS, 0.2% BSA, 0.05% saponin, 5% horse serum) for 40 minutes at RT. Fixed cells were incubated for 40 minutes at RT with a goat anti-rat-AF488 secondary antibody (Invitrogen, Cat# A-11006) in Blocking buffer, to amplify the ICAM-1 signal. After secondary antibody, coverslips were washed with PBS for 5 minutes at RT, and nuclei were stained with Hoechst 33,342 in PBS for 20 minutes at RT. Lastly, coverslips were washed twice with PBS for 2 minutes at RT and mounted with Mowiol 40–88. Confocal microscopy images were acquired and analyzed as previously described.

The average intensity map distribution for ICAM-1 was obtained using a custom-written macro in ImageJ 1.54f. Briefly, single plane images of cDC1 in contact with beads were oriented in the same direction (cell on the left and bead

on the right) and size normalized. Representative images show the average normalized distribution of ICAM-1 obtained by integrating all the normalized cells for each condition. In parallel, the ICAM-1 integrated density at the contact side or the opposed side in each cDC1 were calculated, a normalized by the total ICAM-1 integrated density of the cell.

Statistical analysis

GraphPad Prism version 8 (GraphPad Software Inc.) was used for statistical analysis. Each experiment was independently performed at least thrice. The number of replicates for each experiment is presented in the respective figure legends. Two groups were compared with a two-tailed Student's t-test for paired or unpaired data (when the test assumptions were met). For multiple comparisons, one-way or two-way ANOVA followed by Tukey's posttest (parametric analysis, when the test assumptions were met), or Kruskal-Wallis followed by Dunn's posttest (nonparametric analysis) were used. *p* values <0.05 were considered to be significant.

Further details are described in Supplementary Materials and Methods.

Results

Visualization of cDC1-CD8 T cell contacts in early and late autochthonous KP tumors

To investigate the morphology and distribution of cDC1-CD8 T-cell contacts in the context of progressive lung tumors, we generated a variant of the KP genetic model of NSCLC (*Kras*^{LSL-G12D/+}; *Trp53*^{fl/fl}) by crossing with the *XCR1*^{Venus/+} reporter,²² to unequivocally visualize cDC1 in lung tissues (KP-*XCR1*^{Venus}) (Figure 1a). Lung tumors were induced by intratracheal administration of Cre recombinase and tissues were harvested after 4 weeks (corresponding to early adenomas) and 8 weeks (corresponding to established adenocarcinoma) (Figure S1a). By confocal imaging of lung tissue sections, we observed few sparse Venus⁺ cDC1 distributed in the lung parenchyma. In contrast, in early lung tumors, we detected patches of Venus⁺ cells clustering together (Figure 1b-d). At late time points, the number of cDC1 had diminished and cells were found to be either sparse or clustered at the border of tumor nodules (Figure 1b-d). In parallel, we tracked the evolution of the CD8 T cell compartment at the corresponding time points. CD8 T cells were slightly reduced at late time points and, in line with previous reports, showed a progressive accumulation of exhaustion markers⁴ (Figure S1b, c). Next, we analyzed the number of Venus⁺ cells in contact with CD8 T cells, calculating the maximum angle of the cell-cell interface, as an estimate of the interaction's tightness. In resting lungs, we only captured rare, monogamous cDC1-CD8 T cell conjugates (i.e., featuring 1 DC and 1 T cell) (Figure 1e-f). Remarkably, in tissues carrying early tumors, a large fraction of cDC1 was engaged with CD8 T cells (Figure 1e), often contacting multiple T cells (Figure 1f,g). In contrast, in lungs carrying advanced tumors we detected only a few contacts and most interactions were monogamous and loose (Figure 1e-g).

In summary, these observations in the autochthonous KP-*XCR1*^{Venus} model suggest that lung tissues carrying early tumor lesions promote cDC1-CD8 T cell interactions, whereas advanced tumors are less permissive to contact formation. Since the KP genetic model is inherently poorly immunogenic,^{23,24} the interactions at early time points likely correspond to cDC1-CD8 T cells scanning, before cognate MHC-I TCR recognition.

cDC1 cell-intrinsic changes in advanced lung tumors impair productive DC-T cell interactions

To dissociate tissue factors that may impede DC-T cell encounter in late tumors from cDC1 intrinsic changes impairing contact formation, we next isolated cDC1 from lung tissues to study interaction with CD8 T cells *ex-vivo*. To facilitate the recovery of sufficient numbers of primary cells from tissues and to precisely control the tumor stage, we moved to a transplantable KP line, previously shown to recapitulate most features of autochthonous tumors.^{25,26} Tissues were harvested after 8 or 28 days, corresponding to early dysplasia, or established adenocarcinoma. Cell-sorted cDC1 were pre-pulsed with an OVA class-I peptide (SIINFEKL) to bypass defective antigen uptake and processing and mixed with functional, OVA-specific CD8 T cells (OT-I) (Figure 2a). We used both naïve and effector OT-I, to mimic priming in lymph nodes and secondary interactions in tissue, respectively. cDC1 isolated from early tumors formed significantly more conjugates with naïve OT-I than those isolated from advanced tumors (Figure 2b,c). Furthermore, the surface of interaction (measured as the maximum angle at the interface) and the actin thickness at the interface were significantly diminished in contacts formed with late tumor cDC1, suggesting defects in triggering cytoskeletal remodeling upon contact (Figure 2b,c). A similar pattern was found for effector OT-I, with early tumor cDC1 forming more abundant and stronger conjugates than late tumor cDC1 (Figure S1b), indicating that also interaction with activated CD8 T cells is impaired. These results suggest that in early tumors cDC1 acquire enhanced adhesive properties, which are lost at later stages of tumor progression.

To correlate these observations to the functional outcome of the interaction, we loaded cDC1 *ex vivo* with different concentrations of SIINFEKL to perform assays of CD8 T cell activation. As shown in Figure 2d, we verified that cDC1 isolated from early and late tumors express equal densities of OVA class-I peptide, by staining with 25D-1.16, an antibody specific for peptide: MHC OVA complexes. OT-I cells stimulated by late tumors cDC1 proliferated significantly less than those incubated with early tumors cDC1 (Figure 2e and Figure S1c). Moreover, CD8 T cells primed by late cDC1 produced less IL-2 and IFN γ than those primed by early tumors cDC1 (Figure 2f). Taken together, our results identify two-stages along tumor progression, the first actively promoting productive contacts between cDC1 and CD8 T cells and the second inducing unstable interactions that do not support full T-cell activation.

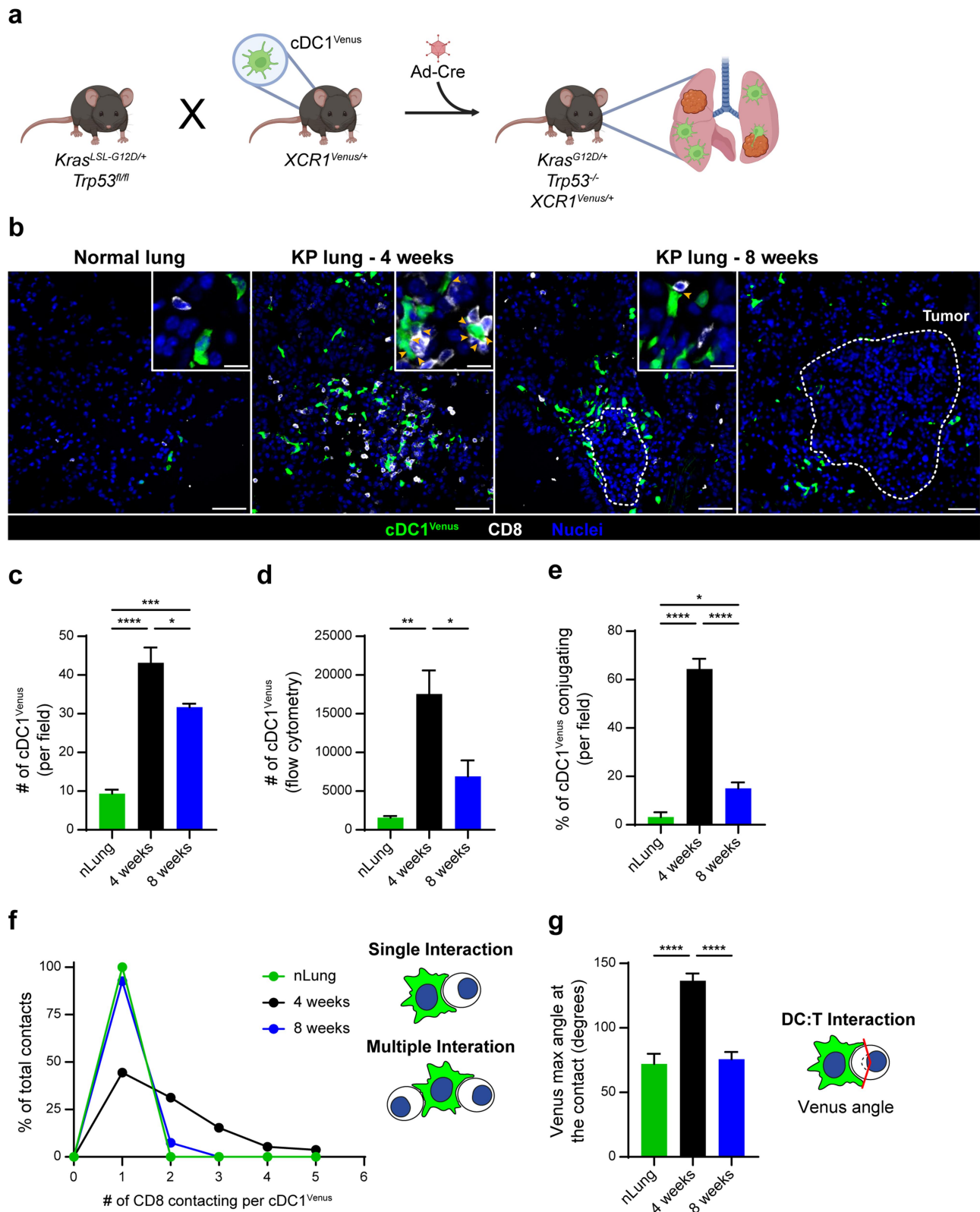


Figure 1. Defective cDC1-CD8 T cell interactions in advanced KP lung tumors. (a) KP mice ($Kras^{LSL-G12D/+}; Trp53^{fl/fl}$) were crossed with the XCR1-Venus reporter ($XCR1^{Venus/+}$) to generate the KP-XCR1^{Venus} line. Tumors were induced by intratracheal Cre-Recombinase Adenovirus (Ad-Cre) administration. (b) Representative confocal planes of 5 μ m lung cryosections from healthy (normal lung) or tumor-bearing lungs (KP) 4- or 8-weeks post Ad-Cre administration. XCR1⁺ cDC1 expressed Venus (green) and CD8 T cells were identified by anti-CD8 antibody labeling (white). Arrows show cDC1-CD8 T-cell interactions. Scale bar large images, 50 μ m; scale bar insets, 6 μ m. (c) Bars show numbers of cDC1^{Venus} in tissue sections (n = 6–8 planes, 3 animals per group). (d) Absolute numbers of cDC1^{Venus} quantified by flow cytometry (n = 3 mice per group, Kruskal–Wallis followed by Dunn’s posttest). (e) Percentage of cDC1^{Venus} engaged in contact with CD8 T cells (n = 6–8 planes, 3 animals per group). (f) The graph shows the multiplicity of cDC1-CD8 interactions in lung tissues. (g) Bars show the maximum angle formed at the interaction interphase (nLung n = 7; 4 weeks n = 42; 8 weeks n = 28, interactions analyzed). One-way ANOVA followed by Tukey’s posttest. Data represent mean \pm SEM, one representative out of three independent experiments is shown. * $p < .05$ ** $p < .01$ *** $p < .001$ **** $p < .0001$.

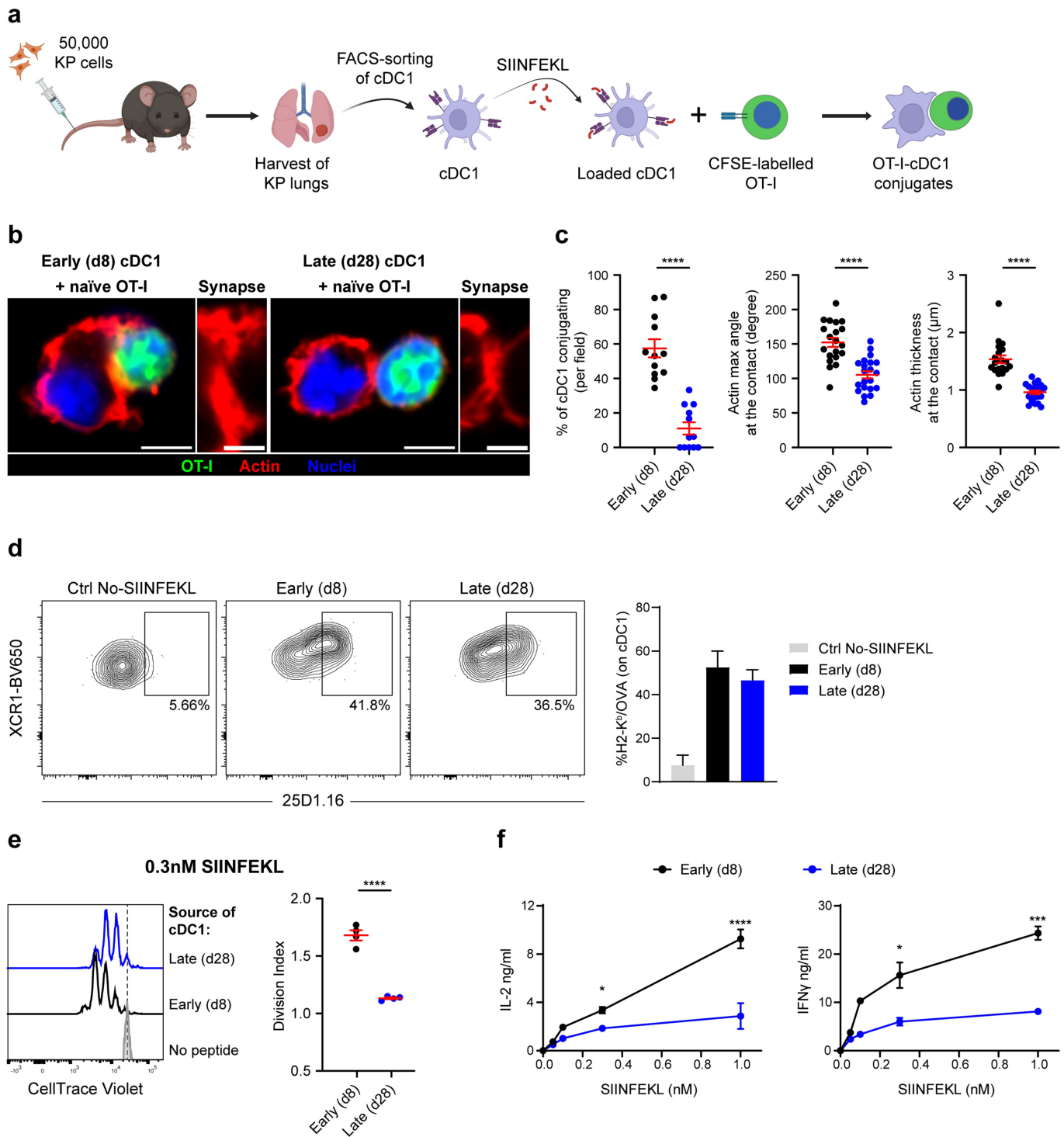


Figure 2. Late tumorconditioned cDC1 fail to establish productive contacts and activate CD8 T cells. (a) Animals were injected intravenously with KP cells to generate tumor nodules in the lung (transplantable model). cDC1 were isolated at day 8 (early) or 28 (late), loaded *ex vivo* with SIINFEKL and mixed with CFSE-labeled OT-I cells to assess IS formation. (b) Representative confocal planes showing cDC1 conjugating with naïve OT-I (scale bar, 4 μm) and the actin structure of the contact site (scale bar, 2 μm). (c) Quantification of the percentage of cDC1 conjugating ($n = 12$ planes per group), the surface of interaction (actin maximum angle) and actin thickness are plotted ($n = 20\text{--}32$ cDC1-OT-I conjugates per group). One-way ANOVA followed by Tukey's posttest. (d) Representative dot plots showing labeling of cDC1 with the MHC I: OVA complex-specific antibody (25D1.16). Percentage of cDC1 expressing the pMHC: OVA complex at early and late stages ($n = 3$ animals per group, one out of two independent experiments). (e-f) cDC1 isolated from KP lungs were loaded *ex vivo* with different concentrations of SIINFEKL and mixed with CTV-labeled OT-I cells. (e) Representative histogram of CTV dilution of OT-I cells and division indexes for each group ($n = 4$ replicates pooled from two independent experiments) after 72 hs of co-incubation (0.3 nM SIINFEKL). Unpaired Student t-test. Unloaded cDC1 (no peptide) were used as negative control for OT-I proliferation. (f) IL-2 and IFN γ produced by OT-I cells after 48 hs of co-incubation, measured by ELISA in the supernatants ($n = 3$ replicates per SIINFEKL concentration). Two-way ANOVA followed by Tukey's posttest. Data represent mean \pm SEM, one representative out of three independent experiments is shown. * $p < .05$ *** $p < .001$ **** $p < .0001$.

Lung tumors induce down-regulation of ALCAM on cDC1

We previously generated a dataset comparing lung resident cDC1 at steady-state to those isolated from advanced lung tumor tissues.³ Focusing on co-stimulatory/co-inhibitory and adhesion molecules that may control interaction with T cells, we identified a set of 45 significantly ($p < 0.05$) expressed genes (20 upregulated, 25 downregulated) (Figure 3a). Adhesion molecules like CD43, ALCAM (CD166), both subunits of LFA-1 (CD18/CD11a) and CD44 were downregulated in late tumor cDC1, which concomitantly upregulated co-inhibitory molecules such as PD-L1 and PD-L2 (Figure 3a). By exploring a publicly available scRNA-seq dataset of KP tumors,² we confirmed the downregulation of ALCAM and the upregulation of PD-L1 and PD-L2 (Figure 3b) in cDC1 associated with advanced tumors. Interestingly, gene expression data indicate that ALCAM is selectively highly expressed in cDC1 of the lung and it is more expressed in cDC1 than in other myeloid lineages (Figure S2a-c).

We then sought to explore ALCAM modulation at the protein level, by flow cytometry on lung cDC1 and migratory cDC1 (CD11c⁺MHC-II^{high}XCR1⁺) in mediastinal lymph nodes (medLNs). We found a significant loss in the expression of ALCAM in lung and migratory cDC1 at late tumor stages, in both the autochthonous (Figure 3c) and transplantable KP models (Figure 3d), which was also mirrored by migratory cDC1 in medLNs. Consistent with RNA seq data, CD44 was reduced in lung late cDC1 in both KP models and PD-L1 and PD-L2 were found to be upregulated. Moreover, MHC-II expression was reduced in late tumors, whilst MHC-I expression was similar in early and late cDC1, ruling out defects in the ability to display antigen to CD8 T cells (Figure S3a, b). These data show that defective contact formation by late tumor cDC1 correlates to diminished expression of adhesion molecules, from which ALCAM stands out, suggesting it may directly control the stability of the interaction.

To extend our findings on ALCAM to human patients, we analyzed ALCAM expression in two publicly available cohorts of lung adenocarcinoma (LUAD) patients. ALCAM was markedly downregulated in primary tumor tissues, as compared to matched noninvolved lung areas from the same patients in both datasets (Figure 3e). Furthermore, patients' stratification into high- and low-ALCAM expression showed a marked overall survival rate difference between the two groups (Figure 3f). Taken together, these results suggest that ALCAM expression is impaired in primary lung lesions and that higher levels of this molecule are associated with better survival outcomes in LUAD patients.

ALCAM triggers contact formation and cytoskeletal rearrangement in early cDC1

ALCAM on monocyte-derived human dendritic cells was shown to bind CD6 on CD4 T cells, regulating T-cell activation.²⁷ To directly investigate the role of ALCAM in primary lung cDC1 during the formation of contacts with CD8 T cells, we isolated XCR1-Venus cDC1 from early KP tumors, loaded cells with SIINFEKL and mixed them with OT-I^{TdTomato}. Confocal imaging using antibodies to label ALCAM showed an even

distribution of the protein on the surface of isolated cDC1. Interestingly, upon contact with T cells, ALCAM preferentially accumulated at the synaptic side of the cell membrane (Figure 4a,b). Next, we developed a reductionist approach to selectively trigger ALCAM on lung cDC1. To this goal, we prepared 6 μ m-polystyrene beads functionalized with a recombinant mouse CD6-Fc chimera, rCD6(Fc), as ligand for ALCAM and rFc-beads as control (Figure 4c). Beads were added to cDC1 isolated from early or late tumor tissues and incubated for 30 minutes before labeling for confocal analysis. Control beads were found in close apposition to the cDC1 surface, without triggering membrane remodeling (Figure 4d,e). Of note, beads carrying rCD6(Fc) triggered membrane deformation and actin recruitment in cDC1 isolated from early tumors (Figure 4d,e). Moreover, rCD6(Fc)-coated beads promoted the mobilization of Intercellular Adhesion Molecule 1 (ICAM-1) to the cDC1-bead contact side (Figure 4f), a crucial step in initiating signaling within IS.⁹ Consistent with the loss of expression of the ligand, and similarly to what was observed with whole CD8 T cells, cDC1 from late tumor-bearing lungs formed significantly fewer contacts with rCD6(Fc)-beads. Moreover, the cDC1-bead surface of the interaction was smaller and flatter and was not enriched in ICAM-1 molecules, resembling that formed by control beads (Figure 4d-f).

Collectively these results suggest that high expression of ALCAM by tissue-resident lung cDC1 promotes stable interaction with CD8 T cells and its loss in advanced tumors correlates to diminished interactions and abortive T-cell activation.

Interfering with ALCAM-CD6 interactions prevents T-cell activation

Finally, we aimed to directly address the functional significance of ALCAM-mediated interactions on CD8 T cell priming by lung cDC1, by probing its role in contact formation and T-cell activation. To this goal, lung cDC1 isolated from early tumor tissues were loaded with SIINFEKL and mixed with naïve OT-I cells, as previously described (Figure 2a). To block the interaction of ALCAM with CD6 ligand on T cells, we added soluble rCD6(Fc) to the co-culture, or soluble rFc as a control. In the presence of rCD6(Fc), cDC1 generated significantly less conjugates with OT-I than in control conditions (rFc) (Figure 4g,h). Moreover, the surface of interaction and the actin thickness at the interface were significantly diminished when ALCAM-CD6 interactions were interfered (Figure 4g,h). Notably, adding rCD6(Fc) to the co-culture led to a significantly reduced IL-2 and IFN γ released by OT-I cells (Figure 4i).

We conclude that blocking ALCAM-CD6 cross-talk impairs the formation of cDC1-CD8 T-cell contacts, supporting a causal link between ALCAM downregulation and inefficient intercellular communication in advanced tumor tissues.

Discussion

The physical interaction between CD8 T cells and cross-presenting cDC1 is a central step in the cancer immune cycle. In addition to interactions occurring in lymph nodes for priming naïve CD8 T cells, secondary interactions in tumor tissues are

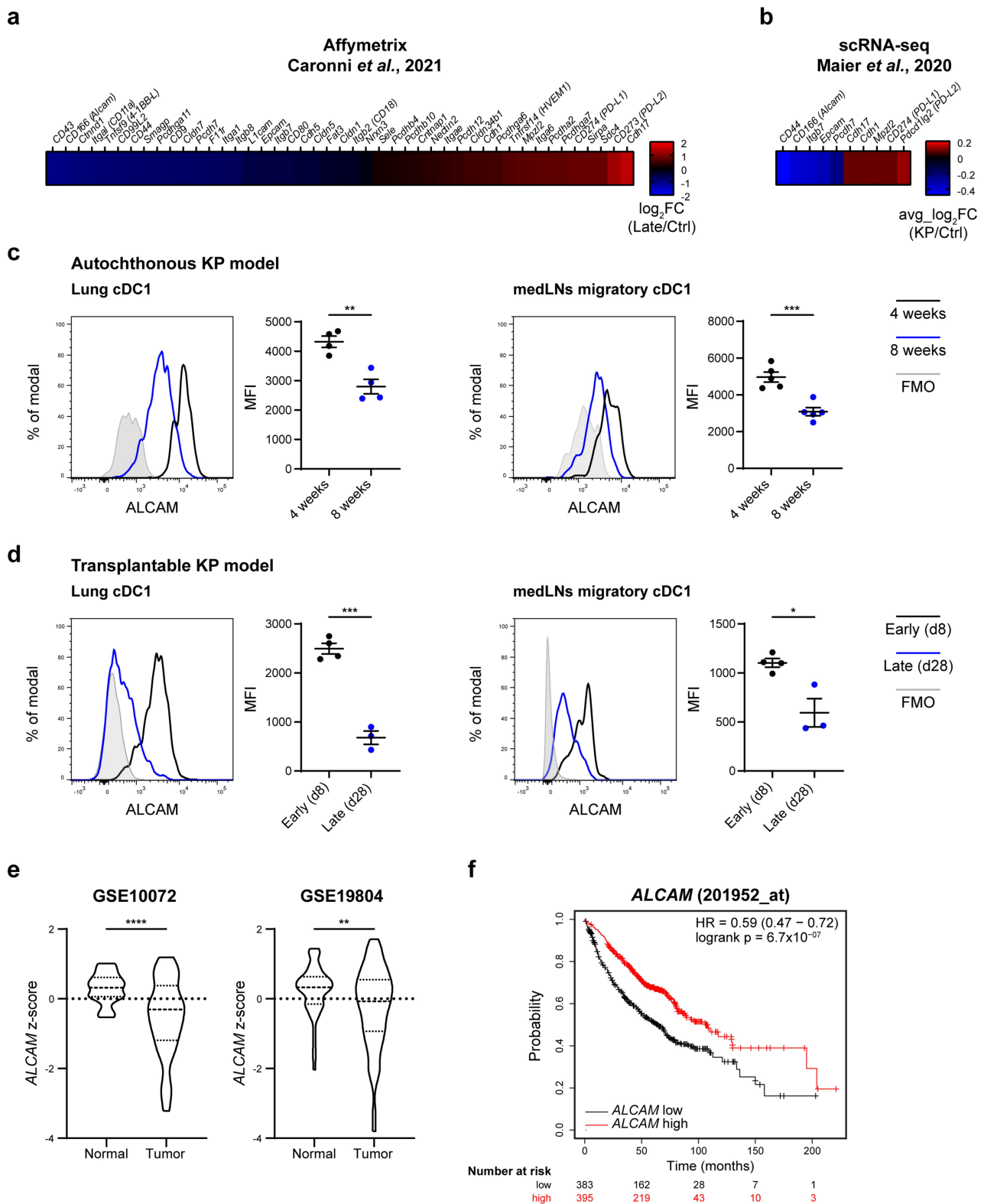


Figure 3. Loss of the adhesion molecule ALCAM in late tumors cDC1. (a) Heatmap showing adhesion molecules differentially expressed ($p < 0.05$) in late KP-bearing lung cDC1 vs control cDC1 (\log_2 Fold Change) in our data set³. (b) Validation of adhesion molecules significantly modulated in late lung cDC1, based on the scRNA-seq dataset from² (average \log_2 Fold Change). (c-d) Lungs and medLNs from tumor-bearing mice were harvested and processed to analyze ALCAM expression by flow cytometry. In the autochthonous model (c), tissues were harvested and analyzed after 4 (black line) or 8 weeks (blue line) post-Ad-Cre administration ($n = 4$ mice per group). In the transplantable model (d), tissues were analyzed at day 8 (black line, $n = 4-5$ mice) or 28 (blue line, $n = 3-4$ mice) after intravenous KP tumor inoculation. ALCAM fluorescence minus one (FMO) control staining is shown in gray. Quantification of the ALCAM Median Fluorescence Intensity (MFI) in each population is presented. Unpaired Student t -test. One representative out of three independent experiments is shown. (e) Violin plots of ALCAM expression in tumor and paired noninvolved tissue (normal) from LUAD patients. GSE10072, $n = 33$; GSE19804, $n = 60$. Paired Student t -test. (f) Survival analysis of LUAD patients. Kaplan–Meier curves of patients stratified by ALCAM expression (low or high). The hazard ratio (HR) and respective 95% confidence interval, as well as the Mantel-Cox (logrank) test are presented. Data represent mean \pm SEM. * $p < .05$ ** $p < .01$ *** $p < .001$ **** $p < .0001$.

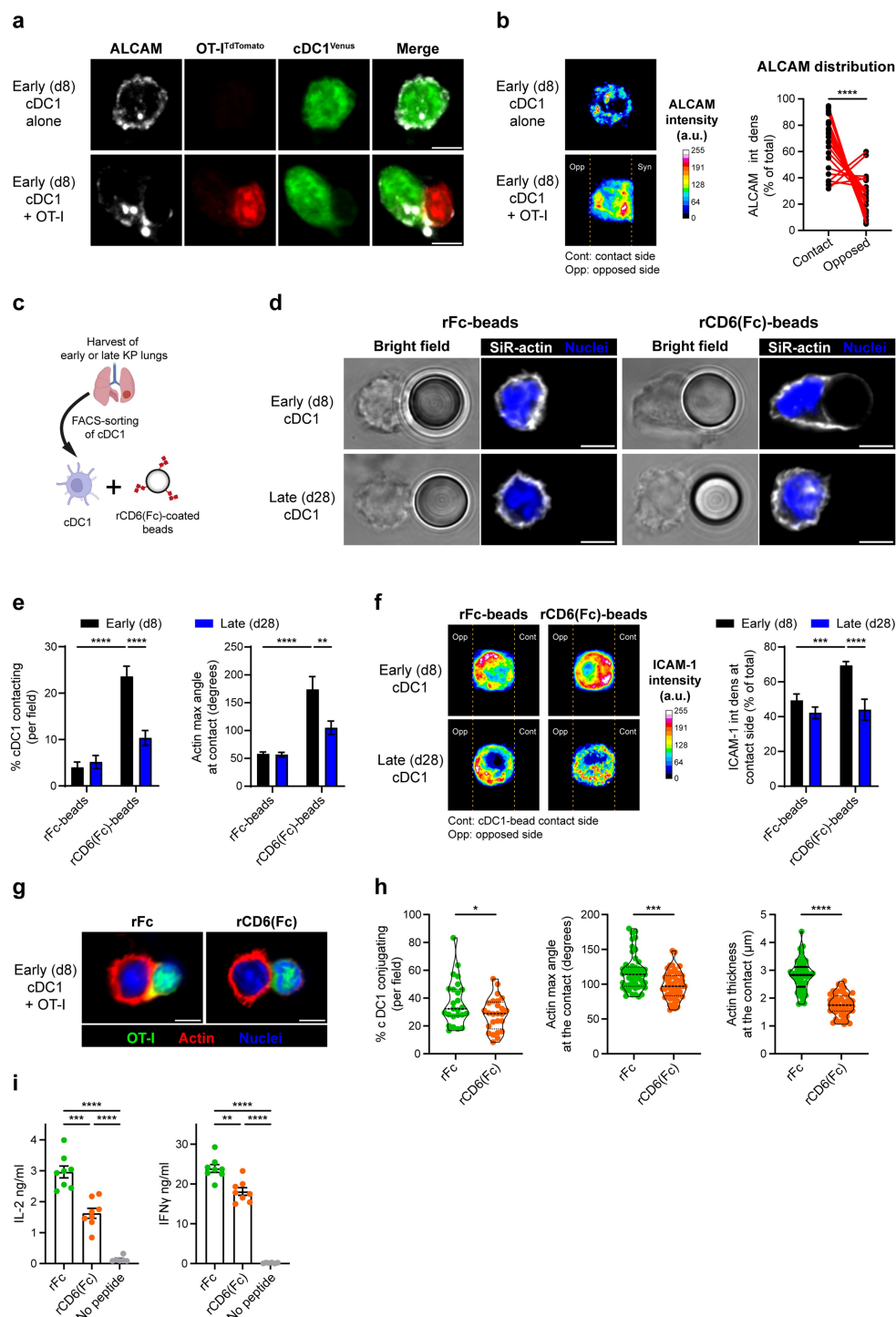


Figure 4. Engaging ALCAM in early cDC1 promotes cytoskeletal rearrangement and sustains CD8 T cell activation. (a) Early (d8) cDC1^{Venus} (green) was loaded *ex vivo* with SIINFEKL and mixed with naive OT-I^{TdTomato} cells (red) on fibronectin-coated coverslips, and subsequently stained for ALCAM (gray). Representative confocal planes showing ALCAM distribution in cDC1 alone (top images) or in cDC1-OT-I conjugates (bottom images) (scale bar, 4 μm). (b) Average intensity map distribution for ALCAM in stacked, size-normalized cDC1 alone (top image) or in contact with OT-I (bottom image, synapse oriented to the right side). Quantification of ALCAM integrated density (int dens) distribution in conjugating cDC1, either at the contact region or at the opposed side ($n = 24$ cDC1-OT-I conjugates). Paired Student t-test. (c-f) 6 μm -beads were functionalized with recombinant rCD6(Fc) (ligand for ALCAM) or rFc as control (c). Isolated cDC1 from early (d8) or late (d28) KP lungs were incubated with beads on fibronectin-coated coverslips. (d) Representative bright field and confocal planes showing cDC1-bead conjugates (scale bar, 4 μm) and SiR-actin (gray) distribution. (e) Quantification of the percentage of cDC1 in contact with beads ($n = 10$ fields per group) and cDC1-bead surface of interaction (actin maximum angle, $n = 10$ cDC1-bead conjugates). (f) Average intensity map distribution for ICAM1 in stacked, size-normalized cDC1 in contact with beads (contact side oriented to the right side). Quantification of the ICAM-1 integrated density at the cDC1-bead contact side (contacts analyzed: $n = 16$ early cDC1-Fc; $n = 16$ early cDC1-rCD(Fc); $n = 15$ late cDC1-Fc; $n = 12$ late cDC1-rCD6(Fc)). In (e-f), Two-way ANOVA followed by Tukey's posttest. (g-i) Isolated lung early (d8) cDC1 was loaded *ex vivo* with SIINFEKL and mixed with naive OT-I cells in the presence of soluble rCD6(Fc) or rFc. (g) Representative confocal planes showing cDC1 conjugating with OT-I cells (scale bar, 4 μm). (h) Quantification of the percentage of cDC1 engaged in contact ($n = 25$ planes per group), the surface of interaction (actin maximum angle) and actin thickness at the contact region ($n = 50$ cDC1-OT-I conjugates per group). Unpaired Student t-test. (i) The cell culture supernatant was collected after 48 hrs of co-incubation to measure the IL-2 and IFN γ secreted by OT-I cells (ELISA) ($n = 8$ replicates pooled from three independent experiments). Unloaded cDC1 (no peptide) was used as negative control for cytokine production. One-way ANOVA followed by Tukey's posttest. Data represent mean \pm SEM, one representative out of three independent experiments is shown. * $p < .05$ ** $p < .01$ *** $p < .001$ **** $p < .0001$.

emerging as critical to regulate anti-tumoral immune responses.²⁸ In this study, focusing on lung tissue-resident cDC1, we show that early steps of carcinogenesis trigger an active scanning behavior *in situ* which results in multiple contacts with CD8 T cells, whereas tissues harboring advanced tumors inhibit intercellular DC-T communication. We have identified ALCAM as a lung-specific cDC1 adhesion molecule facilitating contact formation and signal transmission. Since ALCAM is strongly downmodulated in late tumors, these findings suggest a previously unappreciated additional mechanism of immune evasion.

This study is unique in combining the analysis of cDC1-CD8 T-cell contacts in tissues, to confocal imaging of primary lung cDC1 isolated from tumor tissues during the interaction with CD8 T cells. To facilitate the specific detection of conjugates in lung tissues, we crossed the genetic model of NSCLC⁴ to a cDC1 reporter line.²² This approach has two major advantages. First, it allows the unequivocal identification of cDC1, overcoming the limitations of labeling promiscuous markers (XCR1, CD103, and CD11c) that may be downmodulated during DCs activation. Second, the tumorigenic process occurs *in situ*, recapitulating the correct dynamics of tumor evolution. By quantifying cDC1-CD8 interactions in tissues, we observed a significant increase in clustering at the initial tumor stages, corresponding to early adenomas,²⁹ as compared to healthy lungs. We speculate that sterile inflammation triggered by initial tissue damage and recognition of danger-associated molecular patterns, including cGAS-STING activation, may promote pathways supporting cell-cell encounter and interaction. Since the KP model harbors very few immunogenic antigens,²³ the contacts captured in fixed tissues likely represent events of adhesion molecule-mediated scanning, preceding recognition of cognate antigens and contact stabilization. Therefore, our data suggest that signals in early tumor tissues promote cDC1-mediated scanning of the T cell repertoire, as a mechanism of immune surveillance. In contrast, tissues invaded by adenocarcinomas counteract contact formation and/or maintenance. To understand whether tissue or cDC1-intrinsic factors were primarily responsible for the changes in the capacity to interact, we isolated cDC1 from tumors of different grades to probe the ability to conjugate with CD8 T cells *ex vivo*. Our results strongly suggest that cDC1 cell-autonomous factors contribute to enhanced clustering at early stages and, conversely, failure to stabilize contacts at late stages. Activation of tumor-specific CD8 T cells by cDC1 is a complex, multistep process including antigen capture and cross-presentation, innate sensing to upregulate costimulatory signals, migration to specific niches to convene with CD8 T cells and, finally, engagement in tight physical interactions. Whether the ultimate step of cDC1-CD8 intercellular communication may be modulated across tumor development and by what mechanism, has been little investigated. Both the initial steps of DC-T scanning before TCR-(peptide) MHC recognition and those following TCR engagement are largely controlled by adhesion molecules that facilitate membrane proximity and regulate downstream cytoskeletal remodeling to support intracellular signals.³⁰ Based on our data, we propose the ALCAM-mediated adhesion is crucial to control DC-T scanning in early lung tumors, which is lost in advanced tumors. Intriguingly, the loss of ALCAM is paralleled by the upregulation of inhibitory markers such as PD-L1 and

PD-L2. Therefore, downregulation of ALCAM adds to other known suppressive axes^{2,20,31} to establish a multi-level dysfunctional program in cDC1.

Consistent with our findings, previous studies have demonstrated the importance of the ALCAM-CD6 axis to stabilize interactions with CD4 T cells³² and to promote T-cell priming by human monoDCs.^{27,33,34} Mechanistically, ALCAM has been reported to form a link between CD6 and the actin cortex to strengthen cell adhesion and DC migration,^{32,34} consistent with our observation on actin remodeling. Based on this evidence, we can infer that the loss of ALCAM will impact as well cDC1-CD4 interactions, which we have not addressed in the present study.

In summary, this study introduces the KP-XCR1^{venous} model as a valuable tool to study the spatial localization of cDC1 in lung cancer tissues and provides initial insights into the mechanism that regulates intercellular communication and its suppression during tumor progression.

Acknowledgments

LGM, LL and SJ were supported by ICGEB Arturo Falaschi pre and post-doctoral fellowships. RA is supported by Italian Telethon. We thank Simone Vodret, BioExperimentation Facility Head, ICGEB-Trieste, for technical assistance with the management and manipulation of animal models. We thank Luca Triboli for his support on bioinformatic analysis. Images were created using BioRender.com.

Disclosure statement

No potential conflict of interest was reported by the author(s).

Funding

This work was mainly supported by Associazione Italiana Ricerca Cancro AIRC IG grant 21636 to FB. Additional fundings are from Associazione Italiana Ricerca Cancro IG 22174 and “5 per mille” grant 22759, European Commission [NRRP NextGenerationEU Project CN00000041]; Ministero della Salute [RF-2019-12368718]; Ministero dell’Istruzione, dell’Università e della Ricerca [PRIN-2022XBYNJP, PRIN 2022 PNRR-P2022ZWY8H]; Associazione Italiana per la Ricerca sul Cancro [IG21636].

ORCID

Federica Benvenuti  <http://orcid.org/0000-0002-1908-8052>

Author contributions

LGM and FB conceived the study, designed experiments, and wrote the manuscript. FB supervised the study. LGM performed experiments, data analysis, and prepared the figures. GMP, LL, RA, and SJ assisted in the execution of experiments and critical discussion of the data. LGM and RA analyzed gene expression data. RA wrote custom ImageJ macros for imaging analysis. AR and GDS contributed expertise on the p53-dependent autochthonous lung cancer model. All authors read and approved the final version of the manuscript.

Data availability statement

All data relevant to the study are included in the article or uploaded as supplementary information. They are available upon request from the corresponding author.

References

- Caronni N, Simoncello F, Stafetta F, Guarnaccia C, Ruiz-Moreno JS, Opitz B, Galli T, Proux-Gillardeaux V, Benvenuti F. Downregulation of membrane trafficking proteins and lactate conditioning determine loss of dendritic cell function in lung cancer. *Cancer Res.* 2018;78(7):1685–1699. doi:10.1158/0008-5472.CAN-17-1307.
- Maier B, Leader AM, Chen ST, Tung N, Chang C, LeBerichel J, Chudnovskiy A, Maskey S, Walker L, Finnigan JP, et al. A conserved dendritic-cell regulatory program limits antitumor immunity. *Nature.* 2020;580(7802):257–262. doi:10.1038/S41586-020-2134-Y.
- Caronni N, Piperno GM, Simoncello F, Romano O, Vodret S, Yanagihashi Y, Dress R, Dutertre CA, Bugatti M, Bourdeley P, et al. TIM4 expression by dendritic cells mediates uptake of tumor-associated antigens and anti-tumor responses. *Nat Commun.* 2021;12(1):2237. doi:10.1038/s41467-021-22535-z.
- Schenkel JM, Herbst RH, Canner D, Li A, Hillman M, Shanahan SL, Gibbons G, Smith OC, Kim JY, Westcott P, et al. Conventional type I dendritic cells maintain a reservoir of proliferative tumor-antigen specific TCF-1+ CD8+ T cells in tumor-draining lymph nodes. *Immunity.* 2021;54(10):2338–2353.e6. doi:10.1016/j.immuni.2021.08.026.
- Benvenuti F. The dendritic cell synapse: a life dedicated to T cell activation. *Front Immunol.* 2016;7(MAR):70. doi:10.3389/fimmu.2016.00070.
- Calzada-Fraile D, Sánchez-Madrid F. Reprogramming dendritic cells through the immunological synapse: a two-way street. *Eur J Immunol.* 2023 Aug;53(11):e2350393. doi:10.1002/eji.202350393.
- Comrie WA, Burkhardt JK. Action and traction: cytoskeletal control of receptor triggering at the immunological synapse. *Front Immunol.* 2016;7(MAR):68. doi:10.3389/fimmu.2016.00068.
- Onnis A, Baldari CT. Orchestration of immunological synapse assembly by vesicular trafficking. *Front Cell Dev Biol.* 2019 Jul;7:110. doi:10.3389/fcell.2019.00110.
- Comrie WA, Li S, Boyle S, Burkhardt JK. The dendritic cell cytoskeleton promotes T cell adhesion and activation by constraining ICAM-1 mobility. *J Cell Biol.* 2015;208(4):457–473. doi:10.1083/jcb.201406120.
- Leithner A, Altenburger LM, Hauschild R, Assen FP, Rottner K, Stradal TEB, Diz-Muñoz A, Stein JV, Sixt M. Dendritic cell actin dynamics control contact duration and priming efficiency at the immunological synapse. *J Cell Biol.* 2021;220(4). doi:10.1083/JCB.202006081.
- Benvenuti F, Hugues S, Walmsley M, Ruf S, Fetler L, Popoff M, Tybulewicz VLJ, Amigorena S. Requirement of Rac1 and Rac2 expression by mature dendritic cells for T cell priming. *Science* (1979). 2004;305(5687):1150–1153. doi:10.1126/science.1099159.
- Pulecio J, Petrovic J, Prete F, Chiaruttini G, Lennon-Dumenil AM, Desdouts C, Gasman S, Burrone OR, Benvenuti F. Cdc42-mediated MTOC polarization in dendritic cells controls targeted delivery of cytokines at the immune synapse. *J Exp Med.* 2010;207(12):2719–2732. doi:10.1084/jem.20100007.
- Chiaruttini G, Piperno GM, Jouve M, De Nardi F, Larghi P, Peden AA, Baj G, Müller S, Valitutti S, Galli T, et al. The SNARE VAMP7 regulates exocytic trafficking of interleukin-12 in dendritic cells. *Cell Rep.* 2016;14(11):2624–2636. doi:10.1016/j.celrep.2016.02.055.
- Alcaraz-Serna A, Bustos-Morán E, Fernández-Delgado I, Calzada-Fraile D, Torralba D, Marina-Zárate E, Lorenzo-Vivas E, Vázquez E, de Albuquerque JB, Ruef N, et al. Immune synapse instructs epigenomic and transcriptomic functional reprogramming in dendritic cells. *Sci Adv.* 2021;7(6):eabb9965. doi:10.1126/sciadv.abb9965.
- Cohen M, Giladi A, Barboi O, Hamon P, Li B, Zada M, Gurevich-Shapiro A, Beccaria CG, David E, Maier BB, et al. The interaction of CD4(+) helper T cells with dendritic cells shapes the tumor microenvironment and immune checkpoint blockade response. *Nat Cancer.* 2022;3(3):303–317. doi:10.1038/s43018-022-00338-5.
- Chen JH, Nieman LT, Spurrell M, Jorgji V, Elmelech L, Richieri P, Xu KH, Madhu R, Parikh M, Zamora I, et al. Human lung cancer harbors spatially organized stem-immunity hubs associated with response to immunotherapy. *Nat Immunol.* 2024;25(4):644–658. doi:10.1038/s41590-024-01792-2.
- Magen A, Hamon P, Fiaschi N, Soong BY, Park MD, Mattiuz R, Humblin E, Troncoso L, D'souza D, Dawson T, et al. Intratumoral dendritic cell-CD4(+) T helper cell niches enable CD8(+) T cell differentiation following PD-1 blockade in hepatocellular carcinoma. *Nat Med.* 2023;29(6):1389–1399. doi:10.1038/s41591-023-02345-0.
- Espinosa-Carrasco G, Scivo A, Zumbo P, Dave A, Betel D, Hellmann M, Burt BM, Lee H-S, Schietinger A. Intratumoral immune triads are required for adoptive T cell therapy-mediated elimination of solid tumors. *bioRxiv.* 2023.
- Meiser P, Knolle MA, Hirschberger A, de Almeida GP, Bayerl F, Lacher S, Pedde A-M, Flommersfeld S, Hönninger J, Stark L, et al. A distinct stimulatory cDC1 subpopulation amplifies CD8+ T cell responses in tumors for protective anti-cancer immunity. *Cancer Cell.* 2023;41(8):1498–1515.e10. doi:10.1016/j.ccell.2023.06.008.
- Bayerl F, Meiser P, Donakonda S, Hirschberger A, Lacher SB, Pedde A-M, Hermann CD, Elewaut A, Knolle M, Ramsauer L, et al. Tumor-derived prostaglandin E2 programs cDC1 dysfunction to impair intratumoral orchestration of anti-cancer T cell responses. *Immunity.* 2023;56(6):1341–1358.e11. doi:10.1016/j.immuni.2023.05.011.
- DuPage M, Dooley AL, Jacks T. Conditional mouse lung cancer models using adenoviral or lentiviral delivery of cre recombinase. *Nat Protoc.* 2009;4(7):1064. doi:10.1038/NPROT.2009.95.
- Yamazaki C, Sugiyama M, Ohta T, Hemmi H, Hamada E, Sasaki I, Fukuda Y, Yano T, Nobuoka M, Hirashima T, et al. Critical roles of a dendritic cell subset expressing a chemokine receptor, XCR1. *J Immunol.* 2013;190(12):6071–6082. doi:10.4049/jimmunol.1202798.
- López L, Morosi LG, La Terza F, Bourdely P, Rospo G, Amadio R, Piperno GM, Russo V, Volponi C, Vodret S, et al. Dendritic cell-targeted therapy expands CD8 T cell responses to bona-fide neoantigens in lung tumors. *Nat Commun.* 2024;15(1). doi:10.1038/s41467-024-46685-y.
- Westcott PMK, Muiyas F, Hauck H, Smith OC, Sacks NJ, Ely ZA, Jaeger AM, Rideout WM, Zhang D, Bhutkar A, et al. Mismatch repair deficiency is not sufficient to elicit tumor immunogenicity. *Nat Genet.* 2023;55(10):1686–1695. doi:10.1038/s41588-023-01499-4.
- Herzog BH, Baer JM, Borcherding N, Kingston NL, Belle JL, Knolhoff BL, Hogg GD, Ahmad F, Kang LI, Petrone J, et al. Tumor-associated fibrosis impairs immune surveillance and response to immune checkpoint blockade in non-small cell lung cancer. *Sci Transl Med.* 2023;15(699). doi:10.1126/scitranslmed.adh8005.
- Dimitrova N, Gocheva V, Bhutkar A, Resnick R, Jong RM, Miller KM, Bendor J, Jacks T. Stromal expression of miR-143/145 promotes neoangiogenesis in lung cancer development. *Cancer Discov.* 2016;6(2):188–201. doi:10.1158/2159-8290.CD-15-0854.
- Zimmerman AW, Joosten B, Torensma R, Parnes JR, van Leeuwen FN, Figdor CG. Long-term engagement of CD6 and ALCAM is essential for T-cell proliferation induced by dendritic cells. *Blood.* 2006;107(8):3212–3220. doi:10.1182/blood-2005-09-3881.
- Pittet MJ, Di Pilato M, Garris C, Mempel TR. Dendritic cells as shepherds of T cell immunity in cancer. *Immunity.* 2023;56(10):2218–2230. doi:10.1016/j.immuni.2023.08.014.
- Marjanovic ND, Hofree M, Chan JE, Canner D, Wu K, Trakala M, Hartmann GG, Smith OC, Kim JY, Evans KV, et al. Emergence of a high-plasticity cell state during lung cancer evolution. *Cancer Cell.* 2020;38(2):229–246.e13. doi:10.1016/j.ccell.2020.06.012.
- Martín-Cófreces NB, Vicente-Manzanares M, Sánchez-Madrid F. Adhesive interactions delineate the topography of the immune synapse. *Front Cell Dev Biol.* 2018;6:149. doi:10.3389/fcell.2018.00149.

31. Caronni N, Piperno GM, Simoncello F, Romano O, Vodret S, Yanagihashi Y, Dress R, Dutertre CA, Bugatti M, Bourdeley P, et al. TIM4 expression by dendritic cells mediates uptake of tumor-associated antigens and anti-tumor responses. *Nat Commun.* 2021;12(1):1–15. doi:10.1038/s41467-021-22535-z.
32. Te Riet J, Helenius J, Strohmeyer N, Cambi A, Figdor CG, Müller DJ. Dynamic coupling of ALCAM to the actin cortex strengthens cell adhesion to CD6. *J Cell Sci.* 2014;127(7):1595–1606. doi:10.1242/jcs.141077.
33. Gimferrer I, Calvo M, Mittelbrunn M, Farnòs M, Sarrias MR, Enrich C, Vives J, Sánchez-Madrid F, Lozano F. Relevance of CD6-mediated interactions in T cell activation and proliferation. *J Immunol.* 2004;173(4):2262–2270. doi:10.4049/jimmunol.173.4.2262.
34. Nair P, Melarkode R, Rajkumar D, Montero E. CD6 synergistic co-stimulation promoting proinflammatory response is modulated without interfering with the activated leucocyte cell adhesion molecule interaction. *Clin Exp Immunol.* 2010;162(1):116–130. doi:10.1111/j.1365-2249.2010.04235.x.